ELSEVIER

Biochimica et Biophysica Acta 1418 (1999) 1–18

BIOCHIMICA ET BIOPHYSICA ACTA
BBA

Membrane interactions of the synthetic N-terminal peptide of HIV-1 gp41 and its structural analogs

Patrick W. Mobley [a], Alan J. Waring [b], Mark A. Sherman [c], Larry M. Gordon [b,*]

[a] *Chemistry Department, California State Polytechnic University, Pomona, Pomona, CA, USA*
[b] *Department of Pediatrics, King-Drew Medical Center/UCLA, Los Angeles, CA, USA*
[c] *Physical Biochemistry Section, Division of Biology, Beckman City of Hope Medical Center Duarte, Duarte, CA, USA*

Received 6 October 1998; received in revised form 5 January 1999; accepted 11 January 1999

Abstract

Structural and functional studies assessed the membrane actions of the N terminus of HIV-1 glycoprotein 41 000 (gp41). Earlier site-directed mutagenesis has shown that key amino acid changes in this gp41 domain inhibit viral infection and syncytia formation. Here, a synthetic peptide corresponding to the N terminus of gp41 (FP; 23 residues, 519–541), and also FP analogs (FP520V/E with Val → Glu at residue 520; FP527L/R with Leu → Arg at 527; FP529F/Y with Phe → Tyr at 529; and FPCLP1 with FP truncated at 525) incorporating these modifications were prepared. When added to human erythrocytes at physiologic pH, the lytic and aggregating activities of the FP analogs were much reduced over those with the wild-type FP. With resealed human erythrocyte ghosts, the lipid-mixing activities of the FP analogs were also substantially depressed over that with the wild-type FP. Combined with results from earlier studies, theoretical calculations using hydrophobic moment plot analysis and physical experiments using circular dichroism and Fourier transform infrared spectroscopy indicate that the diminished lysis and fusion noted for FP analogs may be due to altered peptide-membrane lipid interactions. These data confirm that the N-terminal gp41 domain plays critical roles in the cytolysis and fusion underlying HIV-cell infection.

Keywords: Fusion; Erythrocyte; Human immunodeficiency virus; Acquired immunodeficiency syndrome; Circular dichroism; Fourier transform infrared

Abbreviations: CD, circular dichroism; C/P, cholesterol/phospholipid molar ratio; DMSO, dimethyl sulfoxide; 2D-NMR, two-dimensional nuclear magnetic resonance; ESR, electron spin resonance; FP, HIV amino-terminal peptide 519–541 of gp41 (HIV-1 LAV_{1a} strain); FP527L/R, a FP analog in which Leu-527 is replaced by Arg; FP520V/E, a FP analog in which Val-520 is replaced by Glu; FP529F/Y, a FP analog in which Phe-529 is replaced by Tyr; FPCLP1, a truncated FP peptide 526–541; FPCLP2, a truncated FP peptide 525–541; FTIR, Fourier transform infrared; gp41, glycoprotein 41 000 of HIV-1; gp120, glycoprotein 120 000 of HIV-1; HA_2, influenza virus hemagglutinin protein; HFIP, hexafluoroisopropanol; HIV-1, human immunodeficiency virus, type-1; HIV_{ala-E2}, a N-terminal gp41 peptide analog in which Val-520 is replaced by Glu (HIV-1 HXB-2 strain; 23 residues 519–541); LUV, large unilamellar vesicles; PBS, phosphate buffered saline; P/L, peptide to lipid molar ratio; POPC, 1-palmitoyl-2-oleoylphosphatidylcholine; POPG, 1-palmitoyl-2-oleoylphosphatidylglycerol; R_{18}, octadecyl rhodamine B chloride; RBC, red blood cell; SDS, sodium dodecyl sulfate; SP-3, a N-terminal gp41 analog with 3 amino acids removed (residues 520–522; HIV-1 LAV_{1a} strain); SP-4, a N-terminal gp41 analog with 4 amino acids removed (residues 520–523; HIV-1 LAV_{1a} strain); SUV, small unilamellar vesicles; TFE, trifluoroethanol

* Corresponding author. 13655 B Ruette Le Parc, Del Mar, CA 92014, USA. Fax: (310) 6683407; E-mail: lgordon2@san.rr.com

0005-2736/99/$ – see front matter
PII: S0005-2736(99)00014-0

1. Introduction

Previous findings support the hypotheses that the amino-terminal peptide (FP; 23 amino acid residues 519–541 [1]; Table 1) of glycoprotein 41 000 (gp41) is involved in the fusion processes underlying HIV-1 infection of host cells [2]. In myxoviruses and paramyxoviruses, the fusion site on viral envelope protein is a conserved hydrophobic amino acid sequence at the N terminus of the F_1 protein [3]. Gallaher [4] and Gonzalez-Scarano et al. [5] each noted extensive homologies of these sequences with those of the N terminus of gp41, and suggested that the N-terminal gp41 peptide is similarly involved in the fusion of the HIV-1 envelope with target cells. When the HIV-1 glycoprotein 120 000 (gp120) binds to the lymphocyte CD4 receptor, the N-terminal gp41 peptide is activated, which in turn may attack the host cell surface [2,6,7]. According to one model, the N terminus of gp41 penetrates deeply into the host cell membrane [8], and the viral envelope gp41 acts as a bridge, fusing the target cell surface with the HIV-1 lipid bilayer [9,10]. Experimental support for these hypotheses are site-directed mutagenesis studies showing defective gp41 fusion activity for various modifications in the N-terminal HIV-1 gp41 domain, including substitution of hydrophobic amino acids with polar residues [11–15], replacement of highly conserved Gly residues with Val [16] or deletion of short amino acid sequences [17]. Site-directed mutagenesis of the influenza hemagglutinin protein (HA_2) similarly indicated that several point mutations in the N-terminal domain either abolished or shifted the pH response to fusion [18,19]. Besides overall hydrophobicity, Delahunty et al. [16] suggested that the precise sequence and structure of viral fusion peptides were critical for function.

A complementary experimental approach has been to prepare synthetic peptides based on the known N-terminal gp41 sequence, and to then determine whether the biologic activity attributed to the peptide domain in the virus is also seen with the isolated peptide. For example, synthetic peptides based on the N terminus of HIV-1 gp41 induced leakage of lipid vesicles [20–27]. These studies support the Gallaher [4] proposal that the N-terminal domain of gp41 may be partly responsible for the cytolytic actions of whole HIV-1 virions. Consistent with this hypothesis are the findings that FP lysed both $CD4^+$ (cultured Hut 78 lymphocytes) and $CD4^-$ (human erythrocytes) cells [28]. Addition of N-terminal gp41 peptides to model liposomes also promoted lipid mixing [20,21,23–26,29,30]. With human erythrocytes, FP not only triggers rapid lipid mixing between cell membranes, but also produces multicell aggregates [31]. These data suggest that much of the fusogenic actions of HIV-1 gp41 are retained by the N-terminal peptide.

In view of the likely participation of the N-terminal gp41 region in HIV-1 fusion, it is important to elucidate the structure of this domain. The preferred approach would be to determine its three-dimensional structure using X-ray crystallography of the gp41 protein. Unfortunately, earlier X-ray analyses have been performed only on gp41 proteins lacking the N-terminal region, because full-length gp41 proteins do not form crystals [32–35]. Instead, circular dichroism (CD) and conventional Fourier transform infrared (FTIR) spectroscopy have been used to study the conformation of N-terminal gp41 peptides. These techniques indicated that N-terminal gp41 peptides assume variable proportions of α-helix, β and random conformations in structure-promoting solvents and membrane mimics, depending on solvent polarity, lipid charge, peptide concentration and cation concentrations [8,20,21,23–27,29,30]. Further oriented FTIR spectroscopy of N-terminal gp41 peptide indicated an oblique insertion of the α-helical region into lipid bilayers [23,29]. In addition, methodologies that are more 'residue-specific' than CD and FTIR spectroscopy have been used to define the conformation and topography of N-terminal gp41 peptides in membrane mimics. With FP spin-labeled at either Ala-519 or Met-537 incorporated into lipids, electron spin resonance (ESR) studies indicated that the N-terminal Ala-519 inserted deeply into the membrane bilayer, while Met-537 resided at the aqueous-membrane interface [8]. In a more recent 2D nuclear magnetic resonance (2D-NMR), circular dichroism and molecular modeling investigation of FP in either structure-promoting trifluoroethanol (TFE) or detergent sodium dodecyl sulfate (SDS), Chang et al. [36] reported high levels of α-helix. Specifically, FP in 50% TFE assumed an α-helical conformation for residues Ile-522 to Ala-533, while the corresponding α-helix spanned residues Val-520 to Gly-534 for FP

bound to SDS micelles [37]. In further NMR, fluorescence and ESR studies of FP bound to SDS, Chang et al. [37] observed deep penetration of the amphipathic α-helical segment (residues Gly-524 to Gly-534) into the micellar interior. Despite the above extensive spectroscopic results, there is no generally accepted structural model for how the N-terminal gp41 peptide induces membrane lysis and fusion.

A fundamental concern in any structural and functional investigation of synthetic HIV-1 fusion peptides is whether the activity of the isolated peptide bears any relevance to that of the peptide in the virus. A critical test of the significance of viral fusion peptide activities comes from prior site-directed mutagenesis studies, indicating that modification of key residues in the N-terminal gp41 domain reduced HIV infectivity and syncytia formation [12–15,17]. Here, we explore the membrane interactions of a structurally diverse library of synthetic FP analogs, incorporating some of the above modifications which inhibit gp41 protein fusion. Lytic and fusogenic activities were studied with human erythrocytes, chosen because the red cell bilayer lipid composition, asymmetry and molar cholesterol/phospholipid (C/P) ratio approximates those in both the HIV-1 envelope and target cells [9]. We report diminished lytic and fusion activities with our suite of FP variants, confirming that the synthetic N-terminal gp41 peptides may be used as a model for the corresponding N-terminal domain in the full-length HIV-1 gp41 protein. Furthermore, theoretical calculations using hydrophobic moment plots [38] and physical studies employing CD and FTIR spectroscopy on FP and FP variants were performed to map the functionally active regions of the N-terminal gp41 peptide, and to define the structural role of critical amino acid residues.

2. Materials and methods

2.1. Materials

Octadecyl rhodamine B chloride (R_{18}) was from Molecular Probes (Eugene, OR). 1-Palmitoyl-2-oleoylphosphatidylcholine (POPC) and 1-palmitoyl-2-oleoylphosphatidylglycerol (POPG) were from Avanti (Alabaster, AL).

The 23-amino acid N-terminal sequence of gp41 (FP; Table 1) of the HIV-1 strain LAV_{1a} was prepared with an ABI 431A peptide synthesizer, and purified as described earlier [39]; FP encompasses amino acid residues 519–541 of HIV-1 gp41 [1]. The following FP variants (Table 1) were similarly prepared: FP520V/E, FP527L/R (designated FP526L/R in Mobley et al. [31]), FP529F/Y, FPCLP1 (residues 526–541), and FPCLP2 (residues 525–541). These FP variants were based on earlier site-directed, mutagenic experiments that led to defective gp41 fusion activity, with FP520V/E and FP527L/R representing the gp41.2 and gp41.9 mutants [12,13], FP529F/Y representing the FP522F/Y mutant [14], and FPCLP1 representing the penv-7RRE mutant [17]. The expected molecular masses of FP and FP variants were obtained by fast-atom bombardment and electrospray mass spectrometry (UCLA Center for Molecular and Medical Sciences Mass Spectrometry). Quantitative amino acid compositions for the peptides were determined at the UCLA Protein Microsequencing Facility.

2.2. Preparation of human red blood cells (RBC) and resealed human RBC ghosts

RBCs were prepared using outdated units from the local blood bank [28]. All units tested negative for

Table 1
Amino acid sequences of the N-terminal peptide (FP) of HIV-1 gp41 and FP variants

FP (N-terminal segment of HIV-1 gp41, residues 519-541[a])	
	NH_2 A V G I G A L F L G F L G A A G S T M G A R S $CONH_2$
FP520V/E (FP variant, Val → Glu at residue 520)	
	NH_2 A **E** G I G A L F L G F L G A A G S T M G A R S $CONH_2$
FP527L/R (FP variant, Leu → Arg at residue 527)	
	NH_2 A V G I G A L F **R** G F L G A A G S T M G A R S $CONH_2$
FP529F/Y (FP variant, Phe → Tyr at residue 529)	
	NH_2 A V G I G A L F L G **Y** L G A A G S T M G A R S $CONH_2$
FPCLP1 (FP variant, residues 526-541)	
	NH_2 F L G F L G A A G S T M G A R S $CONH_2$
FPCLP2 (FP variant, residues 525-541)	
	NH_2 L F L G F L G A A G S T M G A R S $CONH_2$

[a] The numbering sequence of Myers et al. [1] was used for the HIV-1 strain LAV_{1a}; amino acids are indicated by one-letter codes.

antibodies to HIV-1, and hepatitis B and D. Red cells were washed three times in 0.85% NaCl, and packed cells from the last wash were suspended in isotonic (phosphate-buffered saline (PBS)) buffer, consisting of 120 mM NaCl-2.7 mM KCl-10 mM Na_2HPO_4 (pH 7.4). Lysed and resealed RBC ghosts were prepared according to the method of Sze and Solomon [40], with several modifications [31].

2.3. Hemolysis assays of human RBCs

For testing of peptide-induced hemolysis, small aliquots (≤10 μl) of concentrated FP, or FP variants in 50% DMSO were added to 0.5 ml of the isotonic PBS buffer to yield the desired peptide concentration. Aliquots (10 μl) of the packed, washed cells were then added, and after 30 min at 37°C, the suspension was centrifuged at approx. $5000\times g$ for 1.5 min and the supernatant analyzed spectrophotometrically for hemoglobin at 540 nm [28]. Percent lysis was calculated, using a reference of the average of three tubes in which 10 μl of packed cells were incubated in 0.5 ml of distilled water for the duration of the experiment.

2.4. Lipid mixing (fusion assay)

Lipid mixing between red cell membranes was quantitated from the relief of fluorescence self-quenching of the membrane-incorporated fluorescent probe, R_{18}. Fusion of R_{18}-labeled red blood cell ghosts with unlabeled ghosts reduces the membrane surface density of the fluorophore, thereby producing an increase in fluorescence intensity [41].

For lipid-mixing experiments, the resealed ghosts were divided into two equal portions: one aliquot was stored on ice, while the other was incubated with R_{18} for 1 h at room temperature in the dark. R_{18} was added with vigorous vortexing to a final concentration of 1 mole/50 mole lipid [31]. Unincorporated R_{18} was removed by gel filtration on a Sephadex G-75 column (incubation buffer: 120 mM KCl/30 mM NaCl/10 mM Na_2HPO_4/0.1 mM EDTA), and the unlabeled, resealed ghosts were diluted to the same volume as the labeled, resealed ghosts collected from the column.

Fluorescence intensities were recorded using a Perkin-Elmer 650-40 fluorescence spectrophotometer at 37°C. For fusion measurements, zero fluorescence (F_0) was taken as the emission intensity at 590 nm (560 nm, excitation wavelength) of the labeled and unlabeled resealed ghosts (1:1) before the fusion agent is added, and 100% fluorescence (F_{100}) is the corresponding intensity after the incubation medium is made 1% in Triton X-100. F_s represents the fluorescence intensity, measured for a 1:1 mixture of labeled and unlabeled, resealed ghosts on addition of the putative fusion agent for the indicated time. Accordingly, the percent fusion may be defined as

$$\%\ \text{fusion} = 100\times[(F_s - F_0)/(F_{100} - F_0)] \quad (1)$$

2.5. Coulter counter sizing of human erythrocytes

The aggregation state of human red blood cells was assessed with Coulter counter sizing [31]. Aliquots (10 μl) of washed, packed red blood cells were incubated in 0.5 ml PBS with the indicated agent at 37°C for 30 min. Agents were added as described above for hemolysis assays. At the end of the incubation an aliquot of the mixture was diluted 1/50 000 in isotonic PBS in a 20 ml disposable blood vial (Baxter Diagnostics, Irvine, CA). Particle numbers in each of the 15 size ranges were determined with a Coulter Counter-Model ZBI (Coulter Electronics, Hileah, FL), equipped with a stirrer. The total particle volume (V_T) was calculated as the summation, over each of the 15 channels, of the number (N_C) of particles in each channel multiplied by the maximum particle volume (V_{MC}) in each channel. % total volume in each channel ($\%TV_C$) is then defined as:

$$\%\ \text{total volume} = \%TV_C = 100\times[(N_C\times V_{MC})]/V_T] \quad (2)$$

2.6. CD spectroscopy

CD measurements were made with an AVIV 62DS spectropolarimeter (AVIV Associates, Lakewood, NJ), fitted with a thermoelectric temperature controller [42]. For experiments with peptides in either an aqueous or membrane-mimic solvent [43], 10 μM peptides were respectively suspended in PBS or in hexafluoroisopropanol (HFIP):water (7:3, v/v) with 10 mM phosphate, pH 7.4 (i.e., HFIP solution). CD

spectra were then recorded on peptide dispersions in 0.1–0.5 mm light path demountable cells, scanned from 250–260 nm to 195 nm at a rate of 10 nm/min and a sample interval of 0.2 nm [42,44]. The instrument was routinely calibrated with (+)-10-camphorsulfonic acid (1 mg/ml) and a 1 mm path length cell [45], and the ellipticity expressed as the mean residue ellipticity, $[\theta]_{MRE}$ (deg cm^2 $dmol^{-1}$). Peptide sample concentrations were determined from quantitative amino acid analysis (UCLA Microsequencing Facility, Los Angeles, CA). The percentage of α-helix conformation in the peptide was estimated using reference spectra [46].

2.7. FTIR spectroscopy

Infrared spectra were recorded at 25°C using a Mattson Research Series FTIR spectrometer with a DTGS detector, averaged over 64 scans at a resolution of 2 cm^{-1}. For measurements with peptides in a lipid environment, large unilamellar liposomes (LUV) of POPC:POPG (1 mole:1 mole) lipids in PBS (500 nmoles lipid/ml) of approx. 100 nm diameter were prepared freeze thawing five times, followed by fivefold extrusion through polycarbonate filters using a LipoFast apparatus (Avestin, Ottawa, CA) [44]. Peptides were added to the liposome dispersion from the HFIP solution, and allowed to incubate with the liposomes for 1 h. FTIR spectra were measured on the above unchromatographed peptide:liposome mixtures, and also on these peptide:lipid samples passed through a Sephadex G-50 column to remove non-liposome associated peptide. Chromatographed and unchromatographed lipid-peptide samples were dried onto a 50 mm × 20 mm × 3 mm 45° horizontal ATR crystal (Spectral Solutions, Canyon, CA) by nitrogen gas-enhanced evaporation. The ATR crystal with the lipid-peptide film was sandwiched in a chamber fabricated from black anodized aluminum [47], and mounted on the horizontal ATR fitted with a Minco heater strip controlled by an Omega (Stamford, CT) temperature regulator. The lipid-peptide sample was then hydrated for 2 h by passing nitrogen-^2H_2O vapor through ports in the cell body. Martin et al. [23] earlier noted that the peptide concentration is proportional to the area (S_{amide}) of the amide I band (1680–1600 cm^{-1}), while the lipid concentration is proportional to the area ($S_{\nu(C=O)lipid}$) of the lipid ν(C = O) band (1770–1700 cm^{-1}). Accordingly, the peptide/lipid ratio is proportional to the following ratio: $(S_{amide})/(S_{\nu(C=O)lipid})$.

The relative contributions of the various peptide conformations in the lipid film were estimated from analysis of the amide I bands of the chromatographed sample [42]. The spectrum of the lipid film without peptide was subtracted from that of samples with peptide associated with lipid. The amounts of α-helix, turn, β-structure, and disordered conformations were determined by Fourier self-deconvolution for band narrowing and area calculations of component peaks determined with curve fitting software supplied by Mattson and based on procedures described by Kauppine et al. [48]. The frequency limits for the different structures were as follows: α-helix (1662–1645 cm^{-1}), β-sheet (1637–1613 cm^{-1} and 1689–1682 cm^{-1}), β-turns (1682–1662 cm^{-1}) and disordered or random (1645–1637 cm^{-1}) [42].

2.8. Hydrophobic moment analysis

The association of peptide domains with membranes was predicted with hydrophobic moment analysis [38]. The average hydrophobicity (abscissa) is plotted vs. hydrophobic moment (ordinate) for segments assuming either α-helix or β-sheet conformations. The peptide location is then predicted by noting whether the sequence coordinates lie in the membrane surface, transmembrane or globular regions in these hydrophobic moment plots [8,44].

2.9. Molecular modeling

Segments of the N-terminal peptide of HIV-1 (FP) were modeled with Insight II software, version 97.0 (Molecular Simulations, San Diego, CA) running on a Silicon Graphics R10000 Indigo-2 High Impact workstation (Beckman Research Institute of the City of Hope core facility).

3. Results

3.1. Hemolytic actions of FP and FP variants

The lytic actions of the N-terminal peptide of HIV-1 gp41 (FP) and FP variants were examined

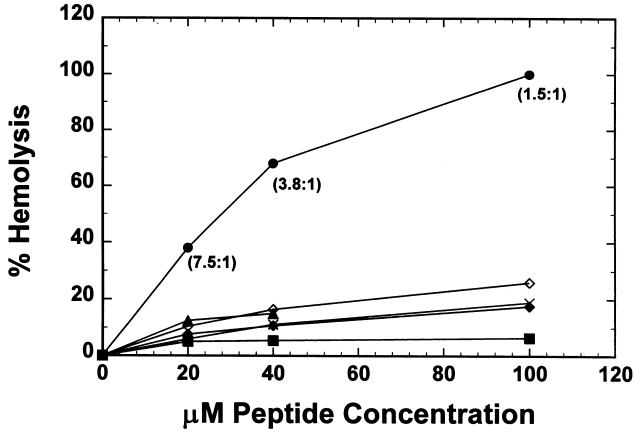

Fig. 1. Dose-dependent effects of the N-terminal peptide of HIV-1 gp41 (FP; ●) and the FP variants FP527L/R (×), FP520V/E (♦), FP529F/Y (▲), FPCLP1 (■) and FPCLP2 (◇) on the isotonic hemolysis of human red blood cells. Amino acid sequences for peptides are shown in Table 1. 'Zero' points for each curve reflect the hemolysis noted with the carrier concentration of DMSO (2.6%). Red cells (1×10^{11} cells/l) were incubated with peptide for 30 min at 37°C. % hemolysis is determined as described in Section 2; 100% hemolysis is defined by incubating 10 μl of packed red cells in 0.5 ml of distilled water for 30 min at 37°C. Numbers in parentheses next to the FP hemolysis curve indicate the lipid:FP molar ratio, calculated assuming quantitative uptake of peptide. Results are reported as the mean of duplicate measurements, and are representative of three independent experiments.

with human red blood cells suspended in an isotonic buffer at 37°C for 30 min. Fig. 1 shows that FP induces a dose-dependent hemolysis, with 40% lysis occurring at 20 μM. If it is assumed that the red cell membrane uptake of FP is quantitative, incubation of 20 μM FP with RBCs will yield a peptide/lipid ratio of approx. 1/7.5 (Fig. 1). Maximal hemolysis of 100% was produced at a higher FP concentration of 100 μM. Previous batches of synthetic FP induced similar lytic results with human red cells [28,31,49]. Control experiments indicate that the highest concentrations of carrier DMSO (i.e., 2.6–5%) did not significantly promote hemolysis. Fig. 1 also shows that the FP variants were much less hemolytic than the wild-type FP for the entire dose range (20–100 μM) tested. To assess the relative inhibitory effects of the amino acid substitutions or deletions in the FP variants, maximal hemolysis (100%) was arbitrarily redefined as that observed after incubating 40 μM FP and erythrocytes for 30 min. Table 2 shows that 40 μM concentrations of each FP variant produced minimal lysis ($\leq$ 23%) when compared to that of FP.

3.2. Lipid-mixing (fusion) actions of FP and FP variants

Fluorescence measurements were carried out to

Table 2
Sequence changes in the N terminus of HIV-1 gp41 reduce the functional activities of the full-length gp41 protein and synthetic FP peptides

Peptide sequence[a]	% of wild-type gp41 protein fusion[b]	% of FP-induced hemolysis[c]	% of FP-induced lipid mixing[d]	% of FP-induced aggregation[e]
FP	100	100	100	100
FP520V/E	< 2[f]	16	58	51
FP529F/Y	4[g]	22	4	35
FP527L/R	< 2[h]	16	8	0
FPCLP1	0[i]	8	0	0
FPCLP2	–[j]	23	0	11

[a]See Table 1 for amino acid sequences of FP and FP variants.
[b]% of wild-type gp41 protein fusion = 100 × [(modified gp41-induced fusion)/(wild-type gp41-induced fusion)].
[c]% of FP-induced hemolysis = 100 × [(% hemolysis with 40 μM peptide)/(% hemolysis with 40 μM FP)] from data in Fig. 1.
[d]% of FP-induced lipid mixing of red cell ghosts = 100 × [(% lipid mixing with 40 μM peptide at 8 min)/(% lipid mixing with 40 μM FP at 8 min)] from data in Fig. 2.
[e]% of 40 μM FP-induced aggregation was determined from Eq. 3 and data in Fig. 3.
[f]gp41 containing Val → Glu at residue 520 [12].
[g]gp41 containing Phe → Tyr at residue 529 [14].
[h]gp41 containing Leu → Arg at residue 527 [12].
[i]gp41 lacking residues 519–525 [17].
[j]Not determined.

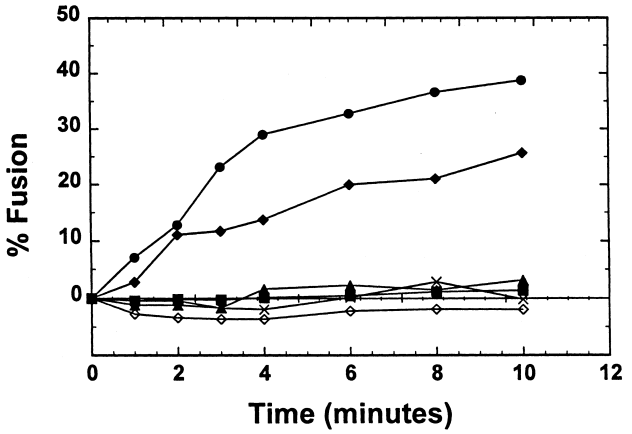

Fig. 2. Time dependence of lipid mixing (fusion) induced by the N-terminal peptide of HIV-1 gp41 (FP), and FP variants using resealed human erythrocyte ghosts at 37°C. Percent fusion is measured by the increase in fluorescence of the lipid-soluble probe, R_{18}, due to relief of self-quenching upon fusion of labeled and unlabeled resealed ghosts (see Section 2). Complete (100%) fusion is taken as the maximal fluorescence resulting from treatment with 1% Triton X-100. R_{18}-labeled (200 μl) resealed ghosts and unlabeled (200 μl) resealed ghosts were incubated with the agent for the indicated times at 37°C in the incubation buffer (pH 7.4; 120 mM KCl/30 mM NaCl/10 mM Na_2HPO_4/0.1 mM EDTA). The total volume was 1.5 ml. The peptides tested were: FP (●), FP527L/R (×), FP520V/E (♦), FP529F/Y (▲), FPCLP1 (■) and FPCLP2 (◇). The peptides were each added to the incubation mixture from a DMSO (100%) stock solution, yielding a 40 μM peptide concentration and 2.6% DMSO. DMSO (2.6%) alone has no effect on lipid mixing [31]. Excitation and emission wavelengths were 560 and 590 nm, respectively. Results are means of duplicate determinations, and are representative of three independent experiments.

determine the lipid-mixing (fusion) effects of FP on resealed erythrocyte ghosts. These assays rely on R_{18} being heavily self-quenched when inserted in a membrane lipid bilayer at high fluorochrome/lipid (approx. 1/100). In the absence of lipid mixing, the dye only very slowly transfers from the bilayers of the labeled resealed ghosts to those of the unlabeled resealed ghosts. When lipid-mixing fusion occurs, the dye is rapidly diluted throughout the system and relief of self-quenching results in an increase in fluorescence. In time-course studies at 37°C, R_{18}-labeled and unlabeled resealed ghosts were incubated with 40 μM FP, and progressively increasing lipid mixing was noted (Fig. 2). Essentially maximum lipid mixing occurred in approx. 7 min. The magnitude and kinetics of FP-induced lipid mixing with resealed human erythrocyte ghosts are comparable to results reported with earlier batches of FP [31]. Control experiments indicated that the highest concentration of carrier solvent (2.6% DMSO) did not promote lipid mixing; the 'zero' time lipid mixing was identical with or without 2.6% DMSO.

Our suite of FP analogs was also investigated for time-dependent effects on lipid mixing between resealed erythrocyte ghosts. Fig. 2 demonstrates that 40 μM FP520V/E promotes lipid mixing, with a similar time-course to that seen with FP; however, the maximal increase in lipid mixing for FP520V/E is significantly less than that observed for FP. With 40 μM concentrations of the FP variants FP527L/R, FP529F/Y, FPCLP1 or FPCLP2, negligible increases in lipid mixing were noted over the time-course of the experiments (Fig. 2). To determine the relative fusogenic activity of the FP and FP variants, maximal lipid mixing (100%) was arbitrarily redefined as that observed after incubating 40 μM FP and erythrocytes for 8 min. Table 2 indicates that the lipid-mixing activity of 40 μM FP520V/E was only 58% of that of FP, and also confirms that 40 μM concentrations of the other FP variants are non-fusogenic.

3.3. RBC aggregating actions of FP and FP variants

Since the above results showed that the FP variants have reduced cytolytic and fusogenic activities compared to those of wild-type FP, the peptides were then tested for aggregation of human red cells. Coulter counter experiments were conducted on washed, packed red cells incubated in isotonic PBS with 40 μM concentrations of FP, FP520V/E, FP527L/R, FP529F/Y, FPCLP1 or FPCLP2 for 30 min. Counts were made for particles in channels ranging in maximum particle volume (μ^3) from 2 to 32 768. Plots of the %(total volume), %TV, versus the maximum particle volume are shown in Fig. 3, where %TV is the percent fraction of the red cell particle volume in a given channel to the total volume of the particles in all channels (see Section 2). For 40 μM FP and carrier DMSO (2.6%), the largest %TV occurred with a maximum particle volume of 256 μ^3 (Fig. 3). Control studies with DMSO (2.6%) alone indicated much smaller particle sizes for red blood cells. Specifically, the 64 μ^3 channel had the largest %TV for red cells treated with only carrier DMSO,

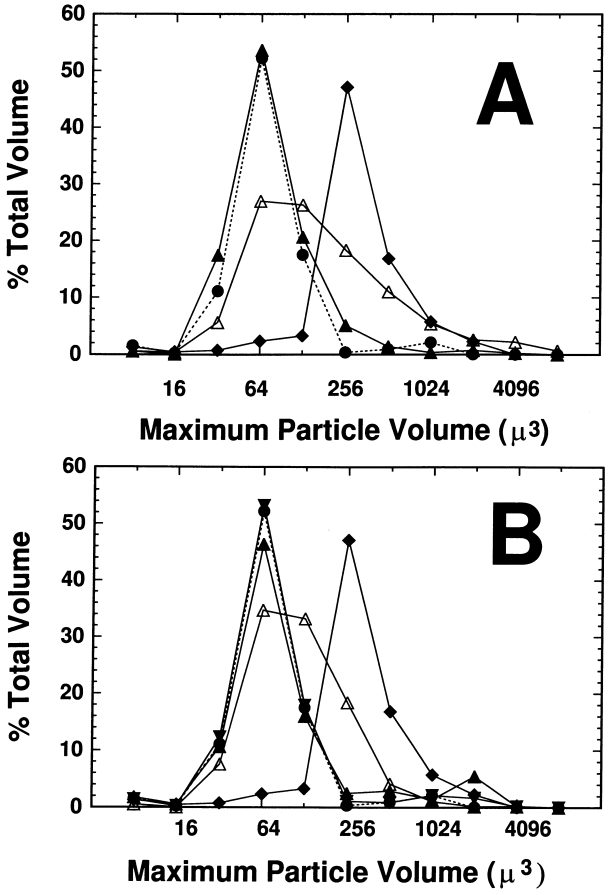

Fig. 3. Coulter counter sizing of erythrocytes treated with the amino terminal peptide of HIV-1 gp41 (FP) and FP variants. Erythrocytes were tested for aggregation by incubating 10 μl of packed red blood cells, diluted to 0.5 ml in PBS buffer, with the following agents at 37°C for 30 min: (A) 40 μM FP and DMSO (2.6%) (♦); 40 μM FP520V/E and DMSO (2.6%) (△); 40 μM FP527L/R and DMSO (2.6%) (▲); and control (2.6% DMSO) (●). (B) 40 μM FP and DMSO (2.6%) (♦); 40 μM FP529F/Y and DMSO (2.6%) (△); 40 μM FPCLP2 and DMSO (2.6%) (▲); 40 μM FPCLP1 and DMSO (2.6%) (▼); and control (2.6% DMSO) (●). At the end of each incubation, an aliquot of the mixture was diluted 1/50 000 in isotonic phosphate-buffered saline. The number of particles in each size range (i.e., maximum particle volume μ^3, x axis) shown was then determined with a Coulter counter. Percent (total volume) for the particles in each channel (y axis) is calculated as in Section 2. Results are means of duplicate determinations, and are representative of three independent experiments.

and represents single cells. FP treatment most likely induces variable aggregations of erythrocytes, with maximum particle volumes greater than 64 μ^3. Single-site substitutions in the amino acid sequence of FP diminished red cell aggregation, with Leu→Arg at 527 (FP527L/R) abolishing red cell aggregation (Fig. 3A), and Val→Glu at 520 (FP520V/E) and Phe→Tyr (FP529F/Y) each reducing the %TV for channels greater than 128 μ^3 (Fig. 3A,B). Removal of either 6 residues (FPCLP2) or 7 residues (FPCLP1) from the N terminus of FP also markedly depressed aggregation; FPCLP1 showed a maximum particle volume distribution similar to that of the DMSO control, while FPCLP2 demonstrated only minimal aggregation above control (Fig. 3B).

The relative aggregating potency of the various FP analogs may be quantified by noting that FP treatment decreases the %TV in the 64 μ^3 channel, in parallel with elevations in the %TV of higher channels (Fig. 3). Since neither FP nor the FP analogs increased the %TV for channels smaller than 64 μ^3 (Fig. 3), the peptides do not grossly fragment red cells. Instead, any decreases in the 64 μ^3 channel reflect reductions in the single cell population caused by peptide-induced cell aggregation. Consequently, decreases in the %TV of the 64 μ^3 channel in Fig. 3 are directly proportional to peptide-induced aggregation. If the %TV in the 64 μ^3 channel induced by 40 μM FP is arbitrarily redefined as that which represents 100% aggregation, then the percentage of FP-induced aggregation for each peptide may then be calculated from:

$$\%\ \text{of FP} - \text{induced aggregation} = 100 \times [(\text{peptide } \%TV_{64}) - (\text{control } \%TV_{64})] / [(\text{FP } \%TV_{64}) - (\text{control } \%TV_{64})] \quad (3)$$

where peptide $\%TV_{64}$, FP $\%TV_{64}$ and control $\%TV_{64}$ are the %(total volumes) in the 64 μ^3 channel induced by FP analog, FP and control, respectively. From Eq. 3, the relative aggregating potency of the peptides decreases in the following order: FP ≫ FP520V/E > FP529F/Y ≫ FPCLP2, FP527L/R, FPCLP1 (Table 2).

3.4. CD spectroscopic analysis of FP and FP variants in a membrane-mimic environment

In light of the above cellular activities of FP and FP variants, it is important to elucidate the respective peptide conformations in membranes and membrane-mimic environments. CD spectroscopy has

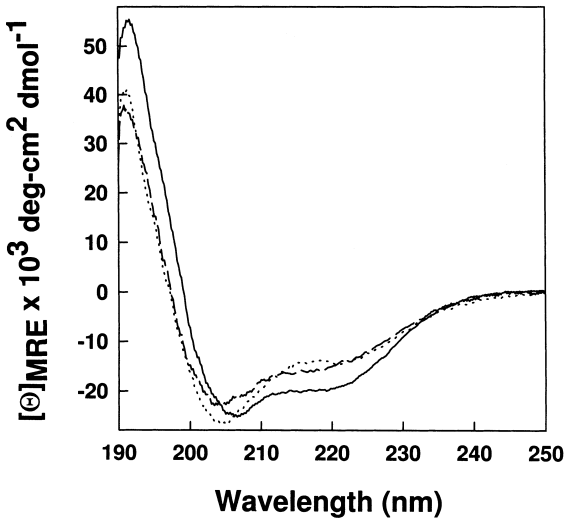

Fig. 4. CD spectra of the N-terminal peptide of HIV-1 gp41 (FP; solid line) and the truncated FP variants FPCLP1 (dotted line) and FPCLP2 (dashed line) in the structure-promoting solvent system, hexafluoroisopropanol:water (7:3, v/v) with 10 mM phosphate, pH 7.4. Peptide concentrations were 10 μM, the temperature was 25°C and the optical path was 5 mm. Spectra represent the average of eight scans.

been previously used to determine the secondary structures of the N-terminal HIV gp41 peptides in a variety of lipid or structure-promoting environments [8,20,22,30,36,37]. Unfortunately, light scattering artifacts preclude similar measurements for CD spectra of FP and FP variants with RBC lipids [8]. Here, CD spectroscopy was used to study FP and FP variants in HFIP:water (7:3, v/v) with 10 mM phosphate, pH 7.4, a membrane-mimic solvent which minimizes light scattering. CD spectra of FP (10 μM) in this solvent indicate considerable α-helix content with a characteristic double minimum at 208 and 220 nm (Fig. 4); quantitatively similar CD spectra (not shown) were obtained for the FP variants FP520V/E, FP527L/R and FP529F/Y when suspended at 10 μM in the HFIP solution. The corresponding spectra of FPCLP1 and FPCLP2 share this double minimum, but show less absorption and are significantly shallower (Fig. 4). Computer analysis of the spectra, using unrestrained least squares fit algorithm and polylysine reference data [50], demonstrated that FP, FP520V/E, FP527L/R and FP529F/Y exhibit approx. 55% α-helix, approx. 45% random structure with no evidence for β-strands. For the 23-amino acid sequence FP and FP variants, these results suggest that approx. 13 residues assume an α-helical conformation. None of the single-site substitutions apparently perturbs the overall peptide conformation in this structure-promoting solvent. Similar analyses of the CD spectra of FPCLP1 and FPCLP2 indicated approx. 45% α-helix, approx. 55% random structure with no β-strands. For the 16-residue FPCLP1 and 17-residue FPCLP2, the CD findings suggest approx. 7–8 residues are α-helical. Since deletion of the N-terminal 6–7 residues in the truncated FP peptides (i.e., FPCLP1 and FPCLP2) reduces α-helical amino acids by 5–6 over that in wild-type FP, the simplest interpretation of these CD results is that the α-helical amino acids encompass the N-terminal residues 519–531, for FP suspended in the HFIP solvent.

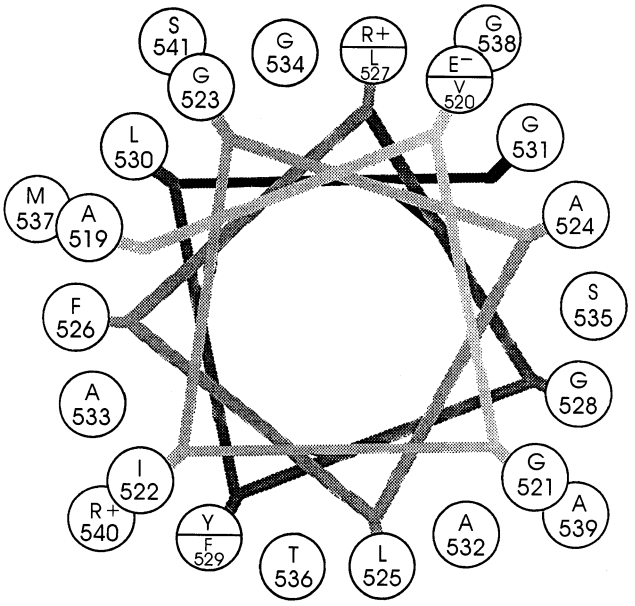

Fig. 5. 'Schiffer-Edmundson' wheel diagrams of the amino-terminal peptide of HIV-1 gp41 (FP) and FP variants [51]. The peptide sequences are indicated by one-letter codes, with amino acid numbering for the wild-type FP from the HIV LAV_{1a} isolate [1]. For the FP520V/E analog, the valine (V) at residue 520 in native FP is replaced by anionic glutamate (E^-). For the FP527L/R analog, the leucine (L) at residue 527 in native FP is replaced by cationic arginine (R^+). For the FP529F/Y analog, the phenylalanine (F) at residue 529 in native FP is replaced by tyrosine (Y). Amino acid residues participating in the α-helix are connected to the barrel projection, while non-participating residues are unattached. These amino acid assignments are from CD spectral results for FP and FP variants suspended at 10 μM concentration in hexafluoroisopropanol:water (7:3, v/v) with 10 mM phosphate, pH 7.4, at 25°C (see Fig. 4 and text).

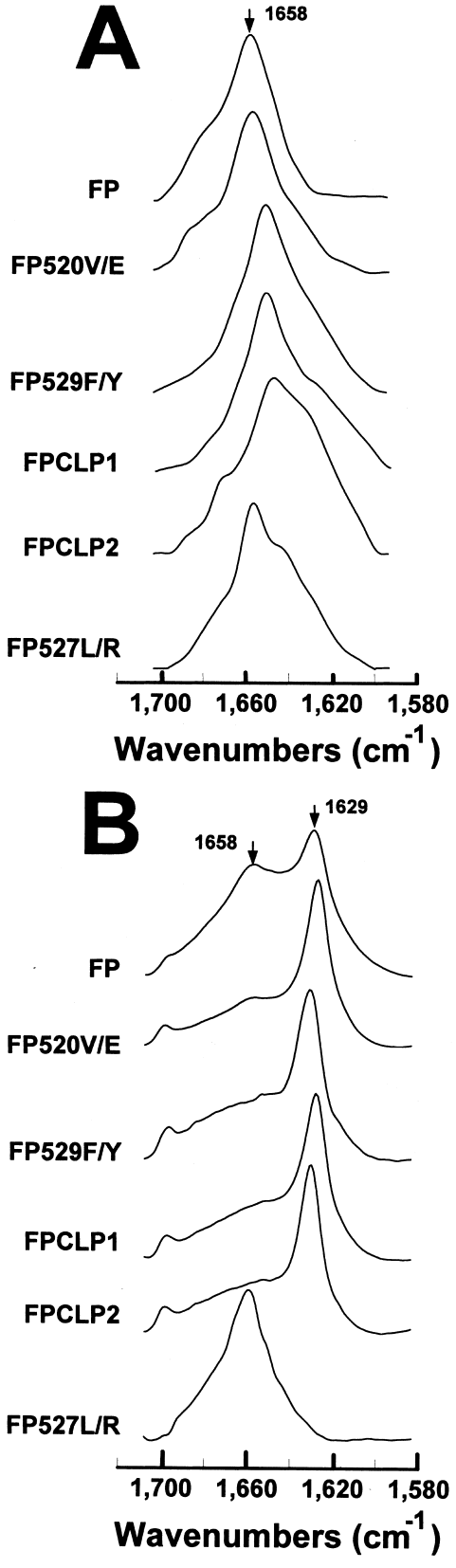

Fig. 6. FTIR spectra of FP and FP variants in POPC:POPG liposomes at lipid/peptide (L/P) ratios of 75 (A) and 10 (B). FP and the FP variants FP520V/E, FP529F/Y, FPCLP1, FPCLP2 and FP527L/R (see Table 1 for amino acid sequences) in a stock solution of HFIP:water (7:3, v/v) with 10 mM phosphate, pH 7.4, were added to LUV of POPC:POPG (1:1) lipids in PBS; FTIR spectra were recorded on peptide:lipid samples chromatographed with a Sephadex G-50 column to remove non-liposome associated peptide. The arrows at 1658 cm^{-1} in A and B indicate the α-helix component, while the arrow at 1629 cm^{-1} in B denotes the β-sheet component.
←

The α-helical structures determined for FP and the FP variants in the HFIP solvent system may be visualized with Schiffer-Edmundson analyses [51]. Fig. 5 is a Schiffer-Edmundson wheel diagram for FP, which shows segregation of a glycine 'stripe' from non-polar residues in two distinct hemifaces, characteristic of an amphipathic sequence capable of transmembrane insertion. The hydrophobic residues (e.g., phenylalanine, isoleucine and leucine) principally lie to the left of the wheel, while the glycine 'stripe' residues primarily lie to the right. Schiffer-Edmundson wheel diagrams for FP520V/E, FP527L/R and FP529F/Y (Fig. 5) indicate that the amino acid substitutions for these three FP variants will each participate in the α-helix. FP520V/E and FP527L/R insert their respective charged residues into the glycine 'stripe' hemiface, while the relatively polar tyrosine replaces the hydrophobic phenylalanine in the non-polar hemiface of FP529F/Y. For the truncated peptides FPCLP1 and FPCLP2 in the HFIP solvent, the residues 525–531 and 526–531 each form respective α-helices (FPCLP1 and FPCLP2 wheel diagrams not shown).

3.5. *FTIR spectroscopic analysis of FP and FP variants in model liposomes*

It is also important to assess the secondary conformations of FP and FP variants in environments that simulate membranes more closely than HFIP solutions, such as LUV of POPC:POPG (1:1) in PBS. Since the zwitterionic POPC and the anionic POPG are comparable to lipids normally found in surface membranes, this mixture should more accurately mimic the lipid bilayer. Unfortunately, CD

spectra of FP and FP variants added to LUV of POPC:POPG (1:1) in PBS indicated substantial spectral noise due to light scattering (spectra not shown), which rendered equivocal measurements of secondary structure (see also [37]). Because of these experimental artifacts, FTIR spectra were next recorded with FP added to large unilamellar lipid vesicles of POPC:POPG (1:1) in PBS. To evaluate the secondary conformation of peptides bound only to POPC:POPG (1:1), FTIR spectra were measured on peptide:lipid samples passed through a Sephadex G-50 column to remove non-liposome associated peptide. For FP added to POPC:POPG (1:1) liposomes at a low initial ratio of peptide/lipid (P/L) of 1/75, Fig. 6A shows the FTIR spectrum of the amide I band, indicating a dominant helical component centered at 1658 cm^{-1}. Subsequent curve fitting of the FP spectrum using the criteria of Susi and Byler [52] confirmed a high proportion of α-helix (1662–1645 cm^{-1}), with much smaller contributions due to β-sheet (1637–1613 cm^{-1} and 1689–1682 cm^{-1}), β-turns (1682–1662 cm^{-1}) and disordered (random) structure (1645–1637 cm^{-1}) (see Table 3). At a higher initial loading (P/L = 1/10), however, the FTIR spectrum of FP (Fig. 6B) showed an additional major band near 1629 cm^{-1} and a relative decrease in the 1658 cm^{-1} band, indicative of predominant β-sheet besides disordered, α-helical and β-turn conformations (Table 3). For N-terminal gp41 peptides with either lipid detergents or model liposomes, FTIR studies have previously reported that the principal secondary conformation shifts from α-helix at low loading to β-sheet at high loading [8,20,29].

Table 3
Proportions of secondary structure for FP and FP variants with POPC:POPG (1:1) LUV liposomes, as estimated from FTIR spectra

Peptide[b]	% conformation for peptide with POPC:POPG liposomes[a]				
	P/L[c]	α-Helix	β-Sheet	β-Turn	Disordered
FP	1/75	60	2	27	11
	1/10	17	40	13	29
FP520V/E	1/75	37	24	19	20
	1/10	31	55	5	10
FP529F/Y	1/75	41	21	23	15
	1/10	0	55	18	27
FP527L/R	1/75	39	16	13	32
	1/10	61	2	26	11
FPCLP1	1/75	45	20	13	22
	1/10	13	58	14	15
FPCLP2	1/75	24	31	15	30
	1/10	5	41	32	22

[a]See Section 2 for determination of percent conformations.
[b]Peptides in a stock solution of HFIP:water (7:3, v/v) with 10 mM phosphate, pH 7.4, were added to LUV of POPC:POPG (1 mole:1 mole) lipids in PBS; FTIR spectra were recorded on peptide:lipid samples chromatographed with a Sephadex G-50 column to remove non-liposome associated peptide.
[c]P/L is the initial peptide to lipid ratio before chromatography of peptide-lipid mixtures.

FTIR spectra were also recorded with FP variants (Table 1) added to POPC:POPG (1:1) liposomes. At low initial P/L ratios of 1/75 for the FP variants, Fig. 6A demonstrates a broad spectral band at approx. 1658 cm^{-1}, similar to that seen with the wild-type, N-terminal HIV-1 gp41 peptide (FP). Spectral deconvolution verified the presence of substantial α-helix structure for each FP variant, although at somewhat lower levels than that noted for FP; significant disordered, α-helical and β-turn conformations were also observed for the FP variants (Table 3). The FP variants FP520V/E, FP529F/Y, FPCLP1 and FPCLP2 each exhibited a conformational shift from high α-helix at low peptide loading (P/L = 1/75) to high β-sheet at high loading (P/L = 1/10), analogous to that noted for native FP (Fig. 6B; Table 3). Of particular interest is the finding that the FP527L/R variant maintains high proportions of α-helical structure and low levels of β-structures, independent of the peptide concentration (Fig. 6A,B; Table 3).

The association of FP and FP variants with POPC:POPG was quantified by recording FTIR spectra, before (not shown) and after chromatographing peptide:lipid mixtures. For POPC:POPG incubated with FP at initial calculated peptide/lipid (P/L) ratios of 1/75 or 1/10, the $(S_{amide})/(S_{\nu(C=O)lipid})$ for unchromatographed and chromatographed samples were similar, indicating quantitative FP uptake (see Section 2). Measurement of these $(S_{amide})/(S_{\nu(C=O)lipid})$ ratios for FP520V/E, FP529F/Y, FPCLP1 and FPCLP2 at initial P/L of 1/75 or 1/10 also showed high peptide binding to lipids, with greater than 75% peptide uptake; contrarily, the chromatographed ratio for FP527L/R was much lower for either P/L of 1/75 or 1/10, indicating less than 25% peptide binding to liposomes at either low or high initial loading.

3.6. Hydrophobic moment plot analysis of membrane interactions with FP and FP variants

The interactions of FP and FP variants with membranes may be further studied using hydrophobic moment plots [38]. Hydrophobic moment plots offer the potential for estimating not only the topographical association of peptides with membranes, but also the degree of peptide self-aggregation [8,53,54]. When a window of 11 residues was earlier used to survey for potential α-helical sequences in wild-type FP [8,53], segments ranging from residues 519–529 to 526–536 had coordinates in the transmembrane sector. Accordingly, these theoretical calculations predicted a deep penetration of the N-terminal HIV-1 gp41 peptide into the membrane bilayer. In the present study with peptides suspended in the membrane-mimic HFIP solvent, we find that FP and the polar amino acid substituted variants form α-helices for the 13-residue sequence 519–531, while the truncated peptides FPCLP1 and FPCLP2 adopt respective α-helices for the 6-residue sequence 526–531 and the 7-residue sequence 525–531 (Figs. 4 and 5). It should also be noted that, at low peptide loading (P/L = 1/75) for FP and FP variants with POPC:POPG liposomes, the dominant conformation was α-helical (Fig. 6A; Table 3). If it is assumed that the α-helical residues are similar in HFIP solution and POPC:POPG at low peptide loading, then hydrophobic moment plots may indicate how the respective α-helical segments interact with membrane bilayers. For α-helical sequences, Fig. 7 predicts that each peptide will bind to membranes, in agreement with our FTIR results with POPC:POPG at a low P/L of 1/75 (Fig. 6A); however, the reduced lipid affinity of FP527L/R noted above may be due to the Leu→Arg substitution forcing the peptide close to the globular-transmembrane multimeric interface (Fig. 7). The polar amino acid substitutions shifted the coordinates for the FP variants into the transmembrane-multimeric zone in Fig. 7, predicting that FP527L/R, FP520V/E and FP529F/Y when membrane-bound will be more aggregated within the lipid bilayer than wild-type FP. Fig. 7 also predicts that FP527L/R and FP520V/E will each reside closer to the polar lipid headgroup, as the respective polar substitutions (Leu→Arg for FP527L/R and Val→Glu for FP520V/E) reduced entry into the hydrophobic interior. The truncated peptides FPCLP1 and FPCLP2 will similarly tend to lie on the membrane surface (Fig. 7).

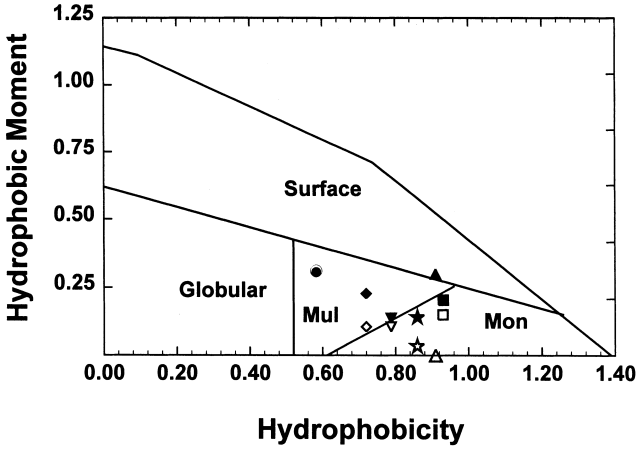

Fig. 7. Hydrophobic moment plot for putative α-helical (closed symbols) and β-sheet (open symbols) sequences of the amino terminal peptide of HIV-1 gp41 (FP) and FP variants, using the computer algorithm of Eisenberg et al. [38]. Hydrophobicity and hydrophobic moments were calculated for: the 13-residue sequence (519–531) of FP (α-helix (★); β-sheet (☆)), FP527L/R (●, ○), FP520V/E (◆, ◇) and FP529F/Y (▼, ▽); the 6-residue sequence (526–531) of FPCLP1 (▲, △); and the 7-residue sequence (525–531) of FPCLP2 (■, □). The α-helix and β-sheet values for FP527L/R are nearly identical. The figure is subdivided into the following membrane regions where the peptide segments are predicted to reside: (i) surface; (ii) Mul, transmembrane multimeric (peptide aggregate); and (iii) Mon, transmembrane monomeric [38]. The globular region denotes peptide segments of low hydrophobic moment and hydrophobicity that are less likely to be membrane associated.

Hydrophobic moment plots may also be used to evaluate the membrane interactions of FP and FP variants at high loading. As the P/L ratio is increased from 1/75 to 1/10, FTIR spectral analysis indicates that the predominant conformation was converted from α-helix to β-sheet for FP and the FP variants FP520V/E, FP529F/Y, FPCLP1 and FPCLP2. If it is assumed as a first approximation that those amino acid residues participating in α-helix at low P/L assume β-sheet conformations at high P/L, then hydrophobic moment plots may be used to study membrane lipid-peptide interactions at high loading. Using a 13-residue window for the FP sequence 519–531, Fig. 7 predicts a deep penetration of the potential β-sheet segment into the membrane interior, but that FP prefers to exist as a monomer. The corresponding β-sheet sequences for FP520V/E and

FP529F/Y also indicate deep insertion into the membrane interior, with equal propensities for monomeric/multimeric states (Fig. 7). Unlike the surface membrane location estimated for the α-helical sequences of FPCLP1 or FLPCLP2 (Fig. 7), the β-sheet conformations for these sequences are predicted to insert into the membrane bilayer as monomers (Fig. 7). Of particular interest is the FTIR finding that the FP527L/R variant retains its high α-helical proportions, regardless of the P/L ratio (Table 3). Accordingly, FP527L/R is predicted to lie close to the globular-transmembrane multimeric interface, assuming an α-helical conformation for residues 519–531 at both low and high peptide loading (Fig. 7).

4. Discussion

Most models for HIV infection of $CD4^+$ cells postulate an important role for the N-terminal domain of the envelope glycoprotein gp41 [3,6,7,14,55,56]. HIV entry into cells is a two-step process [6], in which the virus binds to cell receptors and then promotes fusion between the lipid bilayers of the viral envelope [9,10] and cell surface. The targeting occurs through viral gp120 interacting with host-cell surface CD4 glycoprotein and one of several coreceptors of the chemokine family [57–59]. The interaction of gp120 with cell receptors may expose cryptic gp41 sites [7,55] such as an activated N-terminal gp41 peptide, which may in turn attack the host-cell surface [60]. Recent X-ray diffraction studies [32–35] were interpreted as indicating that gp41 has a multimeric protein core that presents the N-terminal domain as a trimer, similarly to the low-pH induced conformation of influenza virus HA_2 [61]. This suggests that gp41 shares aspects of the low-pH induced 'spring-loaded' mechanism for HA_2, in which the N-terminal fusion peptide undergoes a major translocation [61,62]. Prior structural studies [8,20,27,37] indicated that synthetic N-terminal gp41 peptide (FP) penetrates deeply into membranes. The envelope gp41, along with possible contributions from gp120 and cell receptors, could act as a 'bridge', linking the target cell surface bilayer (through the N terminus of gp41) with the HIV envelope bilayer (through the embedded transmembrane sequences) [9].

Besides simply tethering the HIV envelope to the host cell, the gp41 N terminus may participate more directly in viral-induced fusion. The synthetic N-terminal gp41 peptide (FP; 23 residues) lyses human red cells (Fig. 1) [28,31,39,49], similarly to that observed for N-terminal gp41 peptides with model liposomes [20–26]. Furthermore, the red cell ghost lipid mixing (Fig. 2) [31] induced by FP is characteristic of a classical fusogen, and is comparable to that reported for N-terminal gp41 peptides and model liposomes [20,22–27,29,30]. Such lipid transfers would be required for the merger between the viral envelope and the host-cell plasma membrane. It should be noted that the lipid mixing seen with synthetic N-terminal gp41 peptides is analogous to that observed with intact HIV and either $CD4^+$ lymphocytes [63] or red cell membranes and model liposomes [64].

Earlier findings indicating the participation of gp120 and gp41 regions outside the N terminus in HIV-cell fusion [14,65–67] prompted us to reassess whether synthetic gp41 peptides are a relevant model for the properties of the N-terminal gp41 domain in the whole virus. Since sequence modifications in the N-terminal domain reduced HIV infectivity and syncytia formation in earlier site-directed mutagenesis experiments [12–15,17], it would be important to learn whether these alterations similarly blunt peptide-induced red cell lysis and fusion. Accordingly, FP analogs were synthesized, in which Leu→Arg at residue 527 (FP527L/R) and Val→Glu at 520 (FP520V/E) (see Table 1). FP527L/R and FP520V/E were chosen because an earlier mutagenic study, using $CD4^+$ HeLa cells transfected with HIV *env* glycoprotein expression vectors, indicated that these replacements strongly inhibited syncytia formation [12] (Table 2). Another FP analog with Phe→Tyr at residue 529 (FP529F/Y; see Table 1) was prepared, because this substitution blocked mutant virus-induced syncytia of SupT1 target cells [14] (Table 2). Last, a FP analog lacking residues 519–525 (FPCLP1; Table 1) was synthesized, since transfection of $CD4^+$ HeLa cells with this deletion mutant eliminated syncytia formation [17] (Table 2).

The red cell membrane perturbations achieved by the above panel of FP analogs were much reduced when compared to those of the wild-type FP. For example, the hemolysis induced by FP527L/R, FP520V/E, FP529F/Y or FPCLP1 was sharply diminished (Fig. 1), and correlated well with the de-

creased fusogenicity of the corresponding mutant glycoproteins (Table 2). The FP analogs also exhibited substantially less fusion activity than that of FP, as indicated by lowered lipid mixing and red cell aggregation. Although our results show that peptide-induced hemolysis, lipid mixing or aggregation may each be used to simulate the activity of the gp41 N terminus in HIV fusion processes, Table 2 suggests that FP-induced hemolysis provides the most accurate model. These results broadly agree with earlier studies contrasting the lysis/fusion induced by the N-terminal gp41 peptides with the fusion activity of the parent glycoprotein. For example, FP causes leakage and lipid mixing of resealed RBC ghosts, as well as aggregation of red cells, while FP527L/R was inactive [31]. Similar to our findings with FP520V/E (Figs. 1 and 2), Pereira et al. [25,27] reported that the Val→Glu substitution at residue 520 (HIV_{ala-E2}) depresses the lytic and lipid-mixing activities of the FP peptide (residues 519–541; HXB-2 strain) with model liposomes. Also in agreement are the results from Kliger et al. [30], who showed that the Val→Glu replacement at residue 520 abolished the lipid-mixing activity of the 33-residue N-terminal gp41 peptide (residues 519–551; LAV_{1a} strain). Last, the leakage induced from model liposomes by the deletion N-terminal gp41 analogs SP-3 and SP-4 (i.e., removal of 3 (residues 520–522) or 4 amino acids (residues 520–523), respectively) was dramatically reduced over that of the wild-type peptide (16 residues; 519–536) [29], in parallel with the depressed syncytia-forming activities of the corresponding mutated gp41 [17]. The above results not only indicate that the highly conserved N-terminal gp41 region participates in key HIV fusion processes, but also that addition of synthetic FP (and FP analogs) to red cells or model liposomes is a useful model for investigating these activities. Additional support for these conclusions is the earlier finding that anti-HIV agents which block the membrane actions of the N-terminal gp41 peptide also reduce viral-mediated fusion [39]. The 'capture' of lytic and fusogenic properties of HIV-1 gp41 by the N-terminal peptide may reflect a general phenomenon for lipid-enveloped viruses, as an analogous fusion peptide has been reported for the influenza virus [18,68–70].

It is important to identify those cell components which interact with the N-terminal HIV-1 gp41 peptide. The present FTIR studies show that FP binds to model lipids, suggesting that the surface lipid is one such target. Earlier physical investigations confirm that N-terminal gp41 peptides associate with liposomes [8,20,23–25,27,29,30]; functional experiments indicate that these peptides also promote lysis and fusion of liposomes [20,22,23,25–27,29,30]. Given that FP binds to liposomes made from red blood cell extracts [8], the N-terminal gp41 peptide may produce red cell lysis (Fig. 1), lipid mixing (Fig. 2) and aggregation (Fig. 3A,B) by interacting with the lipid bilayer. Such peptide-induced perturbations are not simply due to non-specific, 'detergent-like' effects. FP has been shown to aggregate red cells in electron microscopy studies, but does not severely disrupt membranes as would be expected if the peptide simply acted as a chaotropic agent [31]. Moreover, the relatively minor modifications in our FP analogs (Table 1) substantially decreased lysis and fusion, indicating that the N-terminal gp41 peptide requires a highly conserved structure to mediate in vivo lipid perturbations. The results on erythrocytes and lipids presented here suggest that FP-induced cytolysis of $CD4^+$ lymphocytes [28] is similarly due to peptide binding to cell-surface membrane lipid, particularly since the red cell bilayer lipid composition, asymmetry and cholesterol/phospholipid ratio approximate those in lymphocytes [9]. It is tempting to further speculate that the gp41 N terminus in intact HIV will induce analogous lytic and fusogenic activities with $CD4^+$ lymphocytes. The related N-terminal peptide of influenza HA_2 has also been proposed to induce fusion through interactions with membrane lipids [3,68–71].

The CD spectroscopic studies on native and truncated N-terminal gp41 peptides in the membrane-mimic HFIP solution (Fig. 4) permit the assignment of the α-helical domain within the FP sequence (Fig. 5). This technique has previously been used to identify discrete conformations within the N-terminal domain SP-B ($SP\text{-}B_{1-25}$; 25 residues) for peptides suspended in structure-promoting environments [42]. High levels of α-helix were found here for FP in HFIP solution, similarly to that reported earlier for N-terminal HIV gp41 peptides in such membrane mimetics as TFE or SDS [8,22,30,36,37]. Quantitative comparisons between the CD spectra of FP and clipped forms of FP in HFIP solution indicated an

α-helical conformation for residues Ala-519 to Gly-531 (Fig. 5). It is worthwhile to compare these results with those from residue-specific physical techniques. Chang et al. [36,37] observed with 2D-NMR spectroscopy that FP in structure-promoting 50% TFE assumed an α-helical conformation for residues Ile-522 to Ala-533, while the corresponding α-helix is slightly more extensive for FP bound to SDS detergent micelles, spanning residues Val-520 to Gly-534. For FP suspended in HFIP solvent, mass spectrometric analysis of hydrogen/deuterium exchange similarly indicated α-helix for residues Gly-523 to Ala-533 [72]. Molecular modeling of HIV-1 FP (not shown) indicated that the carboxyl terminus of the helix was probably a glycine-based cap at Ala-533 known as the α_L motif [73], characterized by Gly-534 assuming a left-handed conformation and a single hydrogen bond between the $>$N-H at Gly-534 and $>$C=O at Leu-530.

The N-terminal HIV-1 gp41 peptide (FP) assumes α-helical conformations not only in HFIP solution and SDS, but also in model liposomes. With a low N-terminal gp41 peptide/lipid of 1/75 that is non-lytic and non-fusogenic (Figs. 1–3) [20,23–25,27,29,30], FTIR spectra indicate that FP in POPC:POPG has high levels of α-helix (Fig. 6A; Table 3). These results may be considered in light of a review [74] questioning whether viral fusion peptides form helices in membranes. Gallaher et al. [74] raised concerns about the frequency of amino acids in FP (e.g., Gly, Ser) which are helix breaking in soluble proteins. Nevertheless, the present findings agree with earlier CD and FTIR studies showing that N-terminal gp41 peptides may form substantial α-helix in model liposomes and lipid extracts from membranes [8,20,23–25,27,29,37]. The experimental results with FP may be reconciled with the criticisms of Gallaher et al. [74] as follows. Although Gly, Val and Ile are 'helix destabilizers' in soluble proteins [74–76], Li and Deber [75,76] reported that these residues are instead α-helix promoters when incorporated into membranes. The elevated α-helix for FP in liposomes argues that the Gly, Val and Ile residues of FP are drawn into the hydrophobic interior of the lipid bilayer, where they become α-helical. Indeed, deep penetration of N-terminal gp41 peptides into membrane bilayers has been predicted from hydrophobic moment plots (Fig. 7) [8,53] and verified with a range of physical measurements [8,20,27,37]. The residue-specific structure model proposed for FP in the membrane-mimic HFIP solution (Fig. 5) may also account for the α-helical component in FTIR spectra of FP with POPC:POPG at low peptide/lipid (Fig. 6A; Table 3); specifically, FP intercalates deeply into the lipid bilayer as an α-helix (Ala-519 to Ala-533). Such FP-lipid interactions may assist in the docking of HIV-1 to target cells, in which FP extends from viral gp41 to 'hook' the HIV-1 envelope to the lymphocyte surface membrane.

The present FTIR experiments also confirm that HIV-1 FP may assume conformations other than α-helix in lipid environments at high peptide loading. Raising the peptide/lipid from 1/75 to 1/10 converted the principal component from α-helix to β-sheet, for FP incubated with POPC:POPG liposomes (Fig. 6A,B; Table 3). For N-terminal gp41 peptides incubated with either lipid detergents or model liposomes, previous FTIR studies have similarly shown a shift from α-helix at low loading to β-sheet at high loading [8,20,29]. Structural investigations of N-terminal gp41 peptides at high loading are of particular interest, since P/L ratios $> \sim 1/25$ with model liposomes are lytic and fusogenic [20,23–25,27,29,30]. Earlier work with N-terminal gp41 peptides has indicated possible roles for the deep insertion of peptide into lipid bilayers [8,20,27,37], oblique intercalation of helical peptide into membrane lipids [23,29], membrane aggregation of peptides [8,30], or the formation of membrane-associated peptide in β-conformations [8,24,25]. Despite these extensive spectroscopic studies with wild-type N-terminal gp41 peptides, there is no generally accepted model for how FP interactions with membranes produce lysis and fusion.

Our physical studies with FP and FP variants allow us to more rigorously test several of the proposed models for how native HIV-1 FP mediates lysis and fusion. As discussed above, one explanation for FP-induced perturbations is the transformation of membrane-associated α-helix to β-sheet [8,24,25]. Consistent with this model are our results indicating that the functionally inactive FP527L/R (Figs. 1–3) does not form substantial lipid-bound β-sheet at either low or high peptide loading of POPC:POPG

(Fig. 6A,B; Table 3). Nevertheless, further experiments with the other FP variants do not support a functional role for membrane-associated β-sheet. Addition of FP520V/E, FP529F/Y or FPCLP1 to POPC:POPG each indicated high levels of lipid-bound α-helix at a low P/L of 1/75; at a high P/L of 1/10, each FP variant exhibited substantial conversions of lipid-associated α-helix to β-sheet (Fig. 6A,B; Table 3). The shift of lipid-bound α-helix to β-sheet noted for wild-type FP at high loading is similar to that observed with FP variants (Fig. 6A,B; Table 3). Since FP520V/E, FP529F/Y or FPCLP1 each show sharply reduced lysis (Fig. 1) and fusion (Figs. 2 and 3) at high peptide loading, the high lipid-associated β-sheet observed for each FP variant does not promote lysis or fusion. It is reasonable to infer that the global conversion of α-helix to β-sheet noted for wild-type FP (Fig. 6A,B; Table 3) is coincidental with, rather than integral to, peptide-induced lysis and fusion. Two previous FTIR investigations using analogs (i.e., HIV_{ala-E2}, SP-3 and SP-4) of the N-terminal HIV-1 gp41 peptide [27,29] similarly confirm that global shifts of α-helix to β-sheet do not facilitate lysis and fusion.

Together with results from earlier studies [8,20,27,37], the structural and functional experiments presented here indicate an important functional role for deep insertion of the N-terminal HIV-1 gp41 peptide into the membrane bilayer. The depressed fusion and cytolysis reported for FP527L/R may be partly due to the reduced peptide binding to bilayer lipid that was determined from FTIR spectra. Substitution of the positively charged Arg for hydrophobic Leu-527 creates a more soluble, 'globular' peptide in hydrophobic moment plots (Fig. 7). For the low levels of FP527L/R that still bind to lipid (Fig. 6A,B), Fig. 7 predicts that the Arg-substituted peptide will be more restricted to the polar headgroup region of the membrane surface. The net effect of the Leu-527 → Arg replacement is to reduce the deep insertion of FP527L/R into the bilayer, and this may be responsible for depressed activities. The reduced membrane perturbations noted for the FP520V/E variant (Figs. 1–3) may also be due to the inability of this peptide to bury deeply into the bilayer interior. Although both the present FTIR uptake studies (Fig. 6A,B) and earlier investigations [25,27,30] show high liposome uptake of N-terminal gp41 variants with Val-520 → Glu, hydrophobic moment analysis (Fig. 7) predicts that the negatively charged Glu replacement will tend to limit the α-helical FP variant to the polar headgroup region. Pereira et al. [27] experimentally confirmed a surface-membrane location for a Val-520 → Glu substituted N-terminal gp41 peptide, using extrinsic fluorescent probes that monitor the surface and interior of lipid bilayers. Last, the lowered lytic and fusion activities of truncated FPCLP1 and FPCLP2 (Figs. 1–3) may be explained by the Fig. 7 prediction that these are 'surface-seeking' peptides when α-helical, due to the lack of the N-terminal AVGIGA sequence. With similarly truncated N-terminal gp41 peptides (i.e., SP-3 and SP-4), Martin et al. [29] reported α-helical orientations nearly parallel to the lipid bilayer plane. These N-terminal deletions may generate FP variants with amphipathic α-helices lying flat on the membrane surface.

Insertion of the N-terminal HIV-1 gp41 peptide into membrane lipid may represent only a critical, initial step in multi-step lytic or fusion processes. A related phenomenon may be the formation of FP aggregates in lipid bilayers at high peptide loading, as indicated by earlier ESR spectroscopy of membranes incubated with spin-labeled FP [8]. Hydrophobic moment analysis predicts that the amino acid substitutions found in FP520V/E, FP527L/R and FP529F/Y may promote the formation of membrane peptide aggregates, whether the N-terminal region is α-helical or β-sheet (Fig. 7). Membrane-associated FP aggregates have been earlier proposed to act in HIV infection as 'fusion pores', which not only destabilize the lipid bilayer but also trigger fusion between the viral envelope and cell surface [3,6,13,15]. The amino acid substitutions in the N-terminal gp41 domain may here create defective membrane pores, which on the one hand reduce peptide-induced hemolysis and fusion and on the other block gp41-mediated syncytia [12,13,15]. The above models for the membrane activities of the gp41 N terminus should be further tested with physical studies of synthetic FP and FP analogs (e.g., ^{13}C-enhanced FTIR and ESR spectroscopy) that map the conformation, orientation and local environment of individual amino acids [8,42,77].

Acknowledgements

We thank Dr. James Bowie (UCLA) for use of the AVIV 62DS spectropolarimeter, Dr. David Eisenberg for the hydrophobic moment program (MOMENT), and the reviewers for helpful comments. The Beckman Research Institute of the City of Hope core facility was supported by Cancer Center Support Grant P30 CA33572. This study was supported by NIH MBRS Grants GM 08140 (L.M.G., A.J.W.) and GM 53933-02 (P.W.M.). The ABI 431A peptide synthesizer was acquired with NIH Small Equipment Grant GM 50483 (A.J.W., L.M.G.).

References

[1] G. Myers, B. Korber, J.A. Berzofsky, R.F. Smith, G.N. Pavalakis, in: Human Retroviruses and AIDS 1991: a Compilation and Analysis of Nucleic Acid and Amino Acid Sequences, Los Alamos National Lab., Los Alamos, NM, 1991, pp. 11–81.
[2] J.M. McCune, L.B. Rabin, M.B. Feinberg, M. Lieberman, J.C. Kosek, G.R. Reyes, I.L. Weisman, Cell 53 (1988) 55–67.
[3] J. White, Science 258 (1992) 917–924.
[4] W.R. Gallaher, Cell 50 (1987) 327–328.
[5] F. Gonzalez-Scarano, M.N. Waxham, A.M. Ross, J.A. Hoxie, AIDS Res. Hum. Retroviruses 3 (1987) 245–252.
[6] E.O. Freed, M.A. Martin, J. Biol. Chem. 270 (1995) 23883–23886.
[7] T.K. Hart, A. Truneh, P.J. Bugelski, AIDS Res. Hum. Retroviruses 12 (1996) 1305–1313.
[8] L.M. Gordon, C.C. Curtain, Y.C. Zhong, A. Kirkpatrick, P.W. Mobley, A.J. Waring, Biochim. Biophys. Acta 1139 (1992) 257–274.
[9] R.C. Aloia, F.C. Jensen, C.C. Curtain, P.W. Mobley, L.M. Gordon, Proc. Natl. Acad. Sci. USA 85 (1988) 900–904.
[10] L.M. Gordon, F.C. Jensen, C.C. Curtain, P.W. Mobley, R.C. Aloia, Biochim. Biophys. Acta 943 (1988) 331–342.
[11] J. Felser, T. Klimkait, J. Silver, Virology 170 (1989) 566–570.
[12] E.O. Freed, D.J. Myers, R. Risser, Proc. Natl. Acad. Sci. USA 87 (1990) 4650–4654.
[13] E.O. Freed, E.L. Delwart, G.L. Buchschacher Jr., A.T. Panganiban, Proc. Natl. Acad. Sci. USA 89 (1992) 70–74.
[14] L. Bergeron, N. Sullivan, J. Sodroski, J. Virol. 66 (1992) 2389–2397.
[15] G.L. Buchschacher Jr., E.O. Freed, A.T. Panganbian, J. Virol. 69 (1995) 1344–1348.
[16] M.D. Delahunty, I. Rhee, E.O. Freed, J.S. Bonifacino, Virology 218 (1996) 94–102.
[17] H. Schaal, M. Klein, P. Gerhmann, O. Adams, A. Scheid, J. Virol. 69 (1995) 3308–3314.
[18] M.-J. Gething, R.W. Doms, D. York, J. White, J. Cell Biol. 102 (1986) 11–23.
[19] D.A. Steinhauer, S.A. Wharton, J.J. Skehel, D.C. Wiley, J. Virol. 69 (1995) 6643–6651.
[20] M. Rafalski, J.D. Lear, W.F. DeGrado, Biochemistry 29 (1990) 7917–7922.
[21] V.A. Slepushkin, G.B. Melikyan, M.S. Sidorova, V.M. Chumakov, S.M. Andreev, R.A. Manukyan, E.V. Karamov, Biochem. Biophys. Res. Commun. 172 (1990) 952–957.
[22] V.A. Slepushkin, S.M. Andreev, M.V. Sidorova, G.B. Melikyan, V.B. Grigoriev, V.M. Chumakov, A.E. Grinfeldt, R.A. Manukyan, E.V. Karamov, AIDS Res. Hum. Retroviruses 8 (1992) 9–18.
[23] I. Martin, F. Defrise-Quertain, E. Decroly, M. Vandenbranden, R. Brasseur, J.-M. Ruysschaert, Biochim. Biophys. Acta 1145 (1993) 124–133.
[24] J.L. Nieva, S. Nir, A. Muga, F.M. Goñi, J. Wilschut, Biochemistry 33 (1994) 3201–3209.
[25] F.B. Pereira, F.M. Goñi, J.L. Nieva, FEBS Lett. 362 (1995) 243–246.
[26] Y.T. Terletskaya, I.O. Trikash, E.S. Serdyuk, S.M. Andreev, Biochemistry (Moscow) 60 (1995) 1309–1314.
[27] F.B. Pereira, F.M. Goñi, A. Muga, J.L. Nieva, Biophys. J. 73 (1997) 1977–1986.
[28] P.W. Mobley, C.C. Curtain, A. Kirkpatrick, M. Rostamkhani, A.J. Waring, L.M. Gordon, Biochim. Biophys. Acta 1139 (1992) 251–256.
[29] I. Martin, H. Schaal, A. Scheid, J.-M. Ruysschaert, J. Virol. 70 (1996) 298–304.
[30] Y. Kliger, A. Aharoni, D. Rapaport, P. Jones, R. Blumenthal, Y. Shai, J. Biol. Chem. 272 (1997) 13496–13505.
[31] P.W. Mobley, H.-F. Lee, C.C. Curtain, A. Kirkpatrick, A.J. Waring, L.M. Gordon, Biochim. Biophys. Acta 1271 (1995) 304–314.
[32] D.C. Chan, D. Fass, J.M. Berger, P.S. Kim, Cell 89 (1997) 263–273.
[33] W. Weissenhorn, A. Dessen, S.C. Harrison, J.J. Skehel, D.C. Wiley, Nature 387 (1997) 426–430.
[34] P.T. Wingfield, S.J. Stahl, J. Kaufman, A. Zlotnick, C.G. Hyde, A.M. Gronenborn, G.M. Clore, Protein Sci. 6 (1997) 1653–1660.
[35] K. Tan, J.-H. Liu, J.-H. Wang, S. Shen, M. Lu, Proc. Natl. Acad. Sci. USA 85 (1997) 12303–12308.
[36] D.-K. Chang, W.-J. Chien, S.-F. Cheng, Eur. J. Biochem. 247 (1997) 896–905.
[37] D.-K. Chang, S.-F. Cheng, W.-J. Chien, J. Virol. 71 (1997) 6593–6602.
[38] D. Eisenberg, R.M. Weiss, T.C. Terwillinger, W. Wilcox, Faraday Symp. Chem. Soc. 17 (1982) 109–116.
[39] L.M. Gordon, A.J. Waring, C.C. Curtain, A. Kirkpatrick, C. Leung, K. Faull, P.W. Mobley, AIDS Res. Hum. Retroviruses 11 (1995) 677–686.
[40] H. Sze, A.K. Solomon, Biochim. Biophys. Acta 550 (1979) 393–406.
[41] D. Hoekstra, T. de Boer, K. Klappe, J. Wilschut, Biochemistry 23 (1984) 5675–5681.

[42] L.M. Gordon, S. Horvath, M.L. Longo, J.A.N. Zasadszinski, H.W. Taeusch, K. Faull, C. Leung, A.J. Waring, Protein Sci. 5 (1996) 1662–1675.
[43] D. Sipos, M. Andersson, A. Ehrenberg, Eur. J. Biochem. 209 (1992) 163–169.
[44] A.J. Waring, S.S.L. Harwig, R.L. Lehrer, Protein Pept. Lett. 3 (1996) 177–184.
[45] W.C. Johnson Jr., Proteins Struct. Funct. Genet. 7 (1990) 205–214.
[46] N. Greenfield, G.D. Fasman, Biochemistry 8 (1969) 4108–4115.
[47] H.S. Matsuzaki, T. Shioyama, I. Okamura, J. Umemura, T. Takenaka, Y. Takashi, T. Fujita, K. Miyajima, Biochim. Biophys. Acta 1070 (1991) 419–428.
[48] J. Kauppine, D. Moffatt, H. Mantsch, D. Cameron, Appl. Spectrosc. 35 (1981) 272–278.
[49] L.M. Gordon, C.C. Curtain, V. McCloyn, A. Kirkpatrick, P.W. Mobley, A.J. Waring, AIDS Res. Hum. Retroviruses 9 (1993) 1145–1156.
[50] M.D. Bruch, M.M. Dhingra, L.M. Gierasch, Proteins Struct. Funct. Genet. 10 (1991) 130–139.
[51] M. Schiffer, A.B. Edmundson, Biophys. J. 7 (1967) 121–135.
[52] H. Susi, D.M. Byler, Biopolymers 25 (1986) 459–487.
[53] R. Brasseur, B. Cornet, A. Burny, M. Vandenbranden, J.M. Ruysschaert, AIDS Res. Hum. Retroviruses 4 (1988) 83–90.
[54] C.C. Curtain, F. Separovic, D. Rivett, A. Kirkpatrick, A.J. Waring, L.M. Gordon, A.A. Azad, AIDS Res. Hum. Retroviruses 10 (1994) 1231–1240.
[55] Q. Sattentau, J. Moore, J. Exp. Med. 174 (1991) 407–415.
[56] C. Wild, J.W. Dubay, T. Greenwell, T. Baird Jr., T.G. Oas, C. McDanal, E. Hunter, T. Matthews, Proc. Natl. Acad. Sci. USA 91 (1994) 12676–12680.
[57] Y. Feng, C.C. Broder, P.E. Kennedy, E.A. Berger, Science 272 (1996) 872–877.
[58] A. Trkola, T. Dragic, J. Arthos, J.M. Binley, W.C. Olson, G.P. Allaway, C. Cheng-Mayer, J. Robinson, P.J. Maddon, J.P. Moore, Nature 384 (1996) 184–187.
[59] L. Wu, N.P. Gerard, R. Wyatt, H. Choe, C. Parolin, N. Ruffing, A. Borsetti, A.A. Cardoso, E. Desjardin, W. Newman, C. Gerard, J. Sodroski, Nature 384 (1996) 179–183.
[60] S. Koenig, V.M. Hirsch, R.A. Olmsted, D. Powell, W. Maury, A. Rabson, A.S. Fauci, R.H. Purcell, P.R. Johnson, Proc. Natl. Acad. Sci. USA 86 (1989) 2443–2447.
[61] P.A. Bullough, F.M. Hughson, J.J. Skehel, D.C. Wiley, Nature 371 (1994) 37–43.
[62] C.M. Carr, P.S. Kim, Cell 73 (1993) 823–832.
[63] F. Sinangil, A. Loyter, D.J. Volsky, FEBS Lett. 239 (1988) 88–92.
[64] C.E. Larsen, S. Nir, D.R. Alford, M. Jennings, K.-D. Lee, N. Düzgünes, Biochim. Biophys. Acta 1147 (1993) 223–236.
[65] J.W. Dubay, S.J. Roberts, B. Brody, E. Hunter, J. Virol. 66 (1992) 4748–4756.
[66] J. Cao, L. Bergeron, E. Helseth, M. Thali, H. Repke, J. Sodroski, J. Virol. 67 (1993) 2747–2755.
[67] S.S. Chen, C.-N. Lee, W.-R. Lee, K. McIntosh, T.-H. Lee, J. Virol. 67 (1993) 3615–3619.
[68] S.A. Wharton, S.R. Martin, R.W.H. Ruigrok, J.J. Skehel, D.C. Wiley, J. Gen. Virol. 69 (1988) 1847–1857.
[69] M.L. Longo, A.J. Waring, D.A. Hammer, Biophys. J. 73 (1997) 1430–1439.
[70] M.L. Longo, A.J. Waring, L.M. Gordon, D.A. Hammer, Langmuir 14 (1998) 2385–2395.
[71] C. Gray, S.A. Tatulian, S.A. Wharton, L.K. Tamm, Biophys. J. 70 (1996) 2275–2286.
[72] A.J. Waring, P.W. Mobley, L.M. Gordon, Proteins Struct. Funct. Genet. Suppl. 2 (1998) 38–49.
[73] R. Aurora, R. Srinivasan, G.D. Rose, Science 264 (1994) 1126–1130.
[74] W.R. Gallaher, J.P. Segrest, E. Hunter, Cell 70 (1992) 531–532.
[75] S.-C. Li, C.M. Deber, Int. J. Pept. Protein Res. 40 (1992) 243–248.
[76] S.-C. Li, C.M. Deber, Struct. Biol. 1 (1994) 368–373.
[77] L. Tadesse, R. Nazarbaghi, L. Walters, J. Am. Chem. Soc. 113 (1991) 7036–7037.